Applied Materials Today 36 (2024) 102072

Contents lists available at ScienceDirect

Applied Materials Today

journal homepage: www.elsevier.com/locate/apmt

Multifunctional graphene quantum dots: A therapeutic strategy for neurodegenerative diseases by regulating calcium influx, crossing the blood-brain barrier and inhibiting Aβ-protein aggregation

I. Jénnifer Gómez [a,b,*], Petra Křížková [c,d], Anna Dolečková [c,d], Lucía Cardo [d], Cecilia Wetzl [d,e], Naděžda Pizúrová [f], Maurizio Prato [d,g,h], Jiřina Medalová [c,*], Lenka Zajíčková [a,i,*]

[a] Department of Condensed Matter Physics, Faculty of Science, Masaryk University, 61137 Brno, Czech Republic
[b] Centro Interdisciplinar de Química e Bioloxía (CICA), Universidade da Coruña, Rúa As Carballeiras, 15071 A Coruña, Spain
[c] Department of Experimental Biology, Faculty of Science, Masaryk University, 62500 Brno, Czech Republic
[d] Center for Cooperative Research in Biomaterials (CIC biomaGUNE), Basque Research and Technology Alliance (BRTA), 20014 Donostia-San Sebastián, Spain
[e] University of the Basque Country, UPV-EHU, 20018 San Sebastián, Spain
[f] Institute of Physics of Materials, Czech Academy of Sciences, 61662 Brno, Czech Republic
[g] Department of Chemical and Pharmaceutical Sciences, University of Trieste, 34127 Trieste, Italy
[h] Ikerbasque, Basque Foundation for Science, 48013 Bilbao, Spain
[i] Central European Institute of Technology - CEITEC, Brno University of Technology, 61200 Brno, Czech Republic

ARTICLE INFO

Keywords:
Carbon dots
Memantine
Protein aggregation
Blood-brain barrier
Bioimaging

ABSTRACT

Multifunctional nanoparticles could be the hallmark for the treatment of neurodegenerative diseases. Dissociation of protein aggregates causing neuronal damage and transfer of specific drugs which can downregulate neuronal excitotoxicity by inhibiting glutamatergic N-Methyl-D-Aspartate-receptors (NMDA) and then reducing calcium influx are among the main factors to consider for proper therapy. Here, we present a multiplatform based on nitrogen-doped graphene quantum dots (NGQDs) with such functionalities. The NGQDs were functionalized with Memantine, the clinically used drug, via covalent and non-covalent coupling, and we confirmed that the pharmaceutical activity was not altered. Apart from that, using xCELLigence technology and flow cytometric analysis of ABC transporter function, we uncovered that the ABC transporters of the blood-brain barrier (BBB) do not affect the ability of NGQD to cross BBB. Surprisingly, this study found that NGQDs have an inhibitory effect on NMDA receptors, thus supporting the action of Memantine. Moreover, NGQDs and their derivatives demonstrated the potential to dissociate β-amyloid aggregates while possessing features suitable for bioimaging in various cell lines.

1. Introduction

Tremendous advances have been made to distinguish and understand the mechanisms that trigger the onset of neurodegenerative diseases in order to find the proper therapy [1]. Nevertheless, up to now, these diseases are incurable and cause progressive loss of brain functions. Despite the different symptoms of these illnesses (*i.e.*, Alzheimer's, Parkinson's, Lewy bodies and dementia, among others), they share common problems, such as neuronal damage that may be caused by protein aggregation [2], and upregulation of neurotransmitters such as glutamate [3]. Overall, neurodegenerative diseases progress is slowed down by therapeutic compounds and one of the most used drugs for treatment of Alzheimer's and other neurodegenerative diseases is 3, 5-Dimethyladamantan-1-amine (Memantine), antagonist of the N-Methyl-d-Aspartate-receptor (NMDA) subtype of glutamate receptor [4]. However, special attention should be paid to the blood-brain barrier (BBB). The BBB prevents the entrance of many therapeutic compounds to the brain from the circulatory system, mainly due to the ATP binding cassette proteins called ABC transporters, which are the challenge for treating brain disorders [5]. There are several methods for drug delivery to target the brain, but most present disadvantages such as high risk, high cost, and lack of compatibility [6]. Likewise, there is an urgent need to develop efficacious therapeutics to prevent the severity of brain function loss and mortality.

* Corresponding authors.
E-mail addresses: i.jennifer.gomez@udc.es (I.J. Gómez), jipro@sci.muni.cz (J. Medalová), lenkaz@physics.muni.cz (L. Zajíčková).

https://doi.org/10.1016/j.apmt.2024.102072
Received 15 October 2023; Received in revised form 22 December 2023; Accepted 11 January 2024
Available online 20 January 2024

In this regard, carbon nanomaterials play a significant role due to their multifunctional properties [6,7]. Carbon nanotubes (CNTs) have emerged as a promising nanocarrier systems and therapeutic agents in many brain-specific therapies [8,9]. More in detail, CNTs were able to cross the BBB easily and also form interfaces with neurons [10,11]. However, CNTs present limitations including their toxicity, no control over CNT length and a high costs of production [12,13]. On the other hand, the anti-neurodegenerative activity of graphene-based materials and carbonaceous zero-dimensional carbon nano-onions was already reported [14–17]. Nevertheless, using those materials in their pristine forms presents some limitations, including the inability to prepare well-dispersed aqueous solutions due to their hydrophobic nature. Thus, further surface modification of these materials is needed for their use in biomedical applications [18].

Carbon dots (CDs), including carbon nanodots, carbon quantum dots, and graphene quantum dots, demonstrate notable advancements within the realm of carbon nanomaterials [19–23]. Their favorable features and promising potential applications have attracted enormous attention since their discovery in 2004 [24–26]. They combine good biocompatibility, low cytotoxicity, water-solubility, unique optical properties, and abundant functional groups (*i.e.*, amino, hydroxyl and carboxyl groups), which make them easy to derivatize [27]. Thus, using CDs might help overcome the limitations discussed above. Besides, various studies have demonstrated the suitability of CDs for bioimaging, drug delivery systems, and, foremost, the ability to cross the BBB both *in vitro* and *in vivo* conditions [7,28–32].

To date, the combination of bioimaging and drug delivery (*i.e.*, detection and treatment) has created unique multiresponse nanoparticles. Here, we report the use graphene quantum dots (GQDs) as brain drug nanocarriers suitable for bioimaging with the ability to cross the BBB and dissociate protein aggregates that cause neurodegenerative diseases. The GQDs were functionalized with Memantine: two different functionalization strategies were evaluated, based on covalent attachment and non-covalent interactions. AFM was employed to assess the synergetic coupling effect and the fibrillation inhibition for the amyloid beta (Aβ) peptide 1–42. The *in vitro* cellular uptake in various cell lines was investigated using confocal fluorescence microscopy. Finally, as a proof-of-principle, we studied the capability of GQDs and their Memantine-functionalized derivatives to cross an *in vitro* model of BBB by real-time cell analysis using xCELLigence technology. Overall, we developed a promising multiresponse nanomaterial that can cross the BBB, detectable by optical spectroscopy methods, and has a dual therapeutic purpose of transferring drugs and dissociating brain protein aggregates.

2. Materials and methods

2.1. Synthetic procedures

2.1.1. NGQDs

NGQDs were synthesized according to our previously reported method [33]. A bottom-up technique in a Discover SP microwave (CEM, USA) with the assisted hydrothermal method was used. Glucose (25 mg, 0.14 mmol.) was dissolved in 1 mL of milli-Q water, followed by the addition of ethylenediamine (21.40 μL, 0.32 mmol). The solution was heated in a microwave reactor at 200 W for 150 s to grow N-GQDs. The N-GQDs samples were filtrated by a microporous filter of 0.1 μm to remove the excess of unreacted compounds. Afterwards, the N-GQDs were dialyzed by molecular weight cut-off of 0.5–1 KDa against pure water for 2 days.

2.1.2. NGQD-Memantine

1-Ethyl-3-(3-dimethylaminopropyl)carbodiimide (EDC, 40 mg, 0.21 mmol) and N-hydroxysuccinimide (NHS, 40 mg, 0.35 mmol) were added to a solution of NGQDs (20 mg) in DMF (5 mL). The mixture was stirred at 0 °C for 1 h. Afterwards, Memantine (20 mg, 0.09 mmol) was added, and the resulting mixture was stirred at room temperature for 16 h. The solvent was removed under reduced pressure, and the crude mixture was dissolved in methanol and isolated by size exclusion chromatography using a column packed with Sephadex LH20 (eluting with methanol). Finally, the solvent was removed under reduced pressure to obtain NGQD-Memantine (18.90 mg) as a brownish powder.

2.1.3. NGQD@Memantine

NGQDs (20 mg) and Memantine (20 mg, 0.09 mmol) were mixture in DMF (5 mL). The mixture was stirred at room temperature for 48 h. The solvent was removed under reduced pressure and the crude mixture was dissolved in methanol and isolated by size exclusion chromatography using a column packed with Sephadex LH20 (eluting with methanol). Finally, the solvent was removed under reduced pressure to obtain NGQD@Memantine (21.50 mg) as a brownish powder.

2.2. Material characterization

AFM images were taken with a Dimension Icon (Bruker, Germany). TEM and high-resolution TEM (HRTEM) images were taken with a JEM 2100F transmission electron microscope (JEOL, Japan). The FTIR spectra were acquired with an Alpha FTIR spectrometer (Bruker, Germany). The XPS was performed with an Axis Supra spectrometer (Kratos Analytical Ltd, UK). The absorption spectra were recorded on a Varian Cary 500 UV–Vis (Agilent Technologies, USA). Fluorescence spectra were measured on a F900 Fluorescent spectrometer (Edinburgh Instruments Ltd, UK). Additional details are given in Supplementary Information.

2.3. Cell-related experiments

2.3.1. BBB model and permeability assay

Transwell plates (CIM-plate, Agilent Technologies, USA) connected to the xCELLigence device (Agilent Technologies, USA) were used for the quantitative kinetic analysis of the BBB formation. The electrode-filters side of wells were pre-coated with 8 μL of 1% porcine skin gelatine (Sigma/Merck) for 1 h at 37 °C and 5% CO_2. Following a similar protocol [34] C8-D1A cells (1.5×10^5 in 162 μL) were seeded on the upside-down turned side of the electrode (further information regarding cell cultivation is placed in Supplementary Information). The astrocyte growth was monitored with the xCELLigence system for 24 h and then the chamber was turned to its original position (upside-down). Afterwards, MS1 cells (1×10^5 in 180 μL) were seeded to the upper chamber and monitoring of their growth continues. When the growth of the cells reached the plateau phase (cell index, Figure S10) in ~24 h, the permeability of the BBB was assed. Then, fresh media containing NGQDs (100 μg/mL), NGQD-Memantine (300 μg/mL), NGQD@Memantine (300 μg/mL), negative control (0.2 μg/mL Streptavidin-Alexa 488) and positive control (20 μg/mL propidium iodide, PI) were added to the upper chamber and the growth of endothelial cells was monitored for further 24 h. Following the time of incubation, the fluorescence of upper and lower chamber was measured by Cytation 5 (BioTek, USA). NGQD and the as-prepared hybrid nanoparticles systems were measured in ex: 390 nm/em: 466 nm, PI was measured in ex: 493 nm/em: 636 nm, Streptavidin-Alexa 488 was measured in ex: 495 nm/em: 519 nm. The rate of diffusion across the membrane, commonly known as permeability coefficient (Papp) was calculated following the next equation (Eq. (1)) [35].

$$P_{app} = \frac{V}{A \times [C]_{apical}} \times \frac{\Delta[C]_{basolateral}}{\Delta t} \quad (1)$$

Where $[C]_{apical}$ is the initial concentration of the as-prepared systems in the apical side; $\Delta[C]_{basolateral}$ is the differential concentration of the as-prepared fluorescent systems in the basolateral side; A: the surface area of membrane; V: volume in basolateral side.

2.3.2. Expression of abc transporters

The isolation of the total RNA was performed using the RNeasy mini kit (Quiagen, Germany) according to the manufacturer's procedure, cell culture details are placed in the Supplementary Information. Briefly, elution of RNA was performed using 42 μL of RNase-free water and its concentration was measured by Nanodrop ND-1000 (Thermo Fisher Scientific).

The reverse transcription reaction (from RNA to cDNA) was performed in the DNA-Engine cycler (Bio-Rad, USA) for 1 h at 42 °C followed by the denaturation of the enzymes for 10 min at 72 °C. The transcription of the mRNA was carried out from the total RNA (1 mg) by using 1 mM Oligo (dT) primer (annealing 65 °C, 5 min, DNA-Engine cycler, Bio-Rad, USA). To 20 μL of RT reaction mixture containing 1 μg of total RNA was added 40 U of RNase inhibitor RiboLock, 1 μM of dNTPs, 200 U of RevertAid reverse polymerase, and 1x Reverse Transcriptase Buffer (all purchased by Thermo Fisher Scientific, USA). 1.5 μL of the as-prepared cDNA was placed in the well of 96 well plate for subsequent quantitative real time PCR. The base of the qPCR reaction mixture was the 0.33xcc LightCycler 480 SYBR green I master kit (Roche, Schwitzerland), 0.375 μM of each primer and 2.125 mM $MgCl_2$. The sequence of forward primer for mABC B1a is 5′-TGGAAGAAGCTAAAAGGCTG-3′, reverse primer for mABC B1a is 5′-CACGGAAAAGAAGACAGTGA-3′. The sequence of forward primer for mABC B1b is 5′-AATCAAAGTGGACCCAACAG-3′, reverse primer for mABC B1b is 5′-CACCAAAGTGAAACCTGGAT-3′. The reaction mixture was preincubated for 5 min at 95 °C, followed by 40 cycles consisting of denaturation 10 s/95 °C, annealing 10 s/60 °C, and extension 10 s/72 °C. Reactions were run in duplicates in the LightCycler® 480 (Roche, Schwitzerland) and melting curves were performed at the end of reaction to check its specificity.

2.3.3. Cell viability – MTT test

Cell viability was measured by using the colorimetric MTT assay (Acros Organics, Geel, Belgium). Cells were seeded (2×10^4) in 96-well-plate (100 μL) and then different concentrations of the as-prepared systems were added and cultivated for 24 h, 48 h, or 72 h. The cells were washed with DMEM medium without Phenol Red (Gibco, Thermo Fisher Scientific) and incubated with 0.5 mg/mL of MTT salt for 3 h at 37 °C and 5% CO_2 followed by 30 min long incubation at room temperature. The MTT-formazan mixture was replaced by 100 μL of DMSO and the absorbance was measured using a micro plate reader at 550 nm (Hidex Sense).

2.3.4. Confocal microscopy

1×10^4 C8-D1A and MS1 cells per well were seeded in μ-Slide 8 Well high Glass Bottom (Ibidi, Grafelfing, Germany) and cultivated overnight. Supernatants were replaced by 100 μL of NGQD (100 μg/mL), NGQD-Memantine (300 μg/mL) and NGQD@Memantine (100 μg/mL) and then incubated for 24 h at 37 °C and 5% CO_2. Afterwards, cells were gently washed by PBS and fixed by 4% paraformaldehyde (Sigma/Merck) for 10 min at room temperature. Lastly, 50 μL of PBS were left in the chamber to avoid cell drying. Images were taken using a confocal microscopy Zeiss LSM 510 (Zeiss, Oberkochen, Germany) using a laser of 405 nm and emission range of 505 nm.

2.4. Inhibition of Aβ1–42 peptides fibrillation

2.4.1. Amyloid β inhibition

The incubation of the fibers was carried out following similar protocols and its preparation is placed in Supplementary Information [36,37]. 25 μM of Aβ1–42 in the absence and presence of NGQDs and their derivatives (22 μg/mL) were incubated for 7 days in constant incubator conditions (37 °C and 5% CO_2, HERAcell). Briefly, aliquots of 20 μL of each sample were placed on a freshly cleaved mica substrate. After incubation for 10 min, the substrate was rinsed twice with water and flow drying with N_2 before measurement. Afterwards, the visualization of Aβ1–42 peptides aggregation with or without NGQDs and the derivatives was performed using a Dimension Icon (Bruker, Germany) in the tapping mode using an RTESPA-150 probe (150 kHz; 6 N/m, Bruker, Germany). The obtained AFM images were analyzed in Gwyddion 2.52 [38]. The area from the agglomerate images was analyzed with ImageJ 1.53t

3. Results and discussion

3.1. Synthesis and characterization of NGQD multifunctional nanoparticles carrying memantine

Nitrogen-GQDS (NGQDs) were prepared following a low-cost, practical bottom-up approach already reported by us (see materials and methods for further details) [33]. The dots are fluorescent and water-soluble nanoplatforms with a quasispherical shape, owning excitation wavelength-dependent multicolor emission and various oxygen and nitrogen functional groups onto the surface, which have shown to be reactive for covalent functionalization [39,40].

Namenda®, known as Memantine, was selected as the neural drug for treating moderate to severe neurodegenerative diseases. As a first functionalization approach, we employed the free amino group of Memantine, which was reactive with the carboxylic groups of NGQDs, using the EDC/Sulfo-NHS coupling agents (Fig. 1). Nevertheless, the amino group modification could affect pharmaceutical activity. Therefore, a second functionalization strategy was designed, based on the non-covalent interactions between the drug and NGQDs [41,42], aiming to evaluate and compare the pharmaceutical activity of these two hybrids.

The feasible routes for preparing the multifunctional platform are depicted in Fig. 1, the neural drug was covalently attached to the carboxylic groups on the NGQD surface via a carbodiimide condensation reaction (further details in materials and methods). Regarding the non-covalent approach, the starting materials were mixed for 48 h to allow formation of hydrogen bonding interactions. Other chemical interactions (*i.e.*, hydrophobic interactions, etc.) might take place. Finally, the systems were purified by size exclusion chromatography (SEC) to remove the excess of NGQDs and Memantine that did not attach to the final hybrid nanoparticles, NGQD-Memantine (covalent approach) and NGQD@Memantine (non-covalent approach).

The size and morphology of the as-prepared hybrid nanoparticles were analyzed by atomic force and transmission electron microscopies (AFM and TEM). From AFM and TEM data, we can infer that the systems maintain a quasispherical morphology and crystal structure after functionalization (Fig. 2a-e and Figures S1 and S2). Concretely, the nanoparticles presented an average size of ~ 3.0 ± 1.1 nm for NGQD-Memantine and ~ 4.2 ± 1.7 nm for NGQD@Memantine (Fig. 2c and Figure S2). We cannot rule out the possibility that some dots may react among themselves through the amines and the activated acids. Nevertheless, size exclusion was used to purify the hybrids and avoid the presumed aggregates, as confirmed through TEM analysis (Fig. 2c and Figure S2).

The chemical structure was characterized using Fourier transform infrared (FTIR) and X-ray photoelectron (XPS) spectroscopies. FTIR spectrum of the NGQD-Memantine and NGQD@Memantine showed the characteristic infrared signals of both NGQDs and Memantine (Fig. 2f). For instance, the C—H from the aliphatic region of Memantine (~3054–2724 cm^{-1}) was observed. Regarding the covalent approach, an increase in the ratio between the amide and amine band was noted in NGQD-Memantine compared to NGQD, *i.e.*, the band at 1655 cm^{-1} corresponding to the amide band increased while at 1537 cm^{-1}, the amine decreased, confirming that Memantine is loaded onto the surface of the dots via an amide bond. Oppositely, in the non-covalent case, we did not observe such a feature.

The studies carried out by XPS demonstrated that the as-prepared hybrid nanoparticles contained mainly elemental carbon (78.1 and

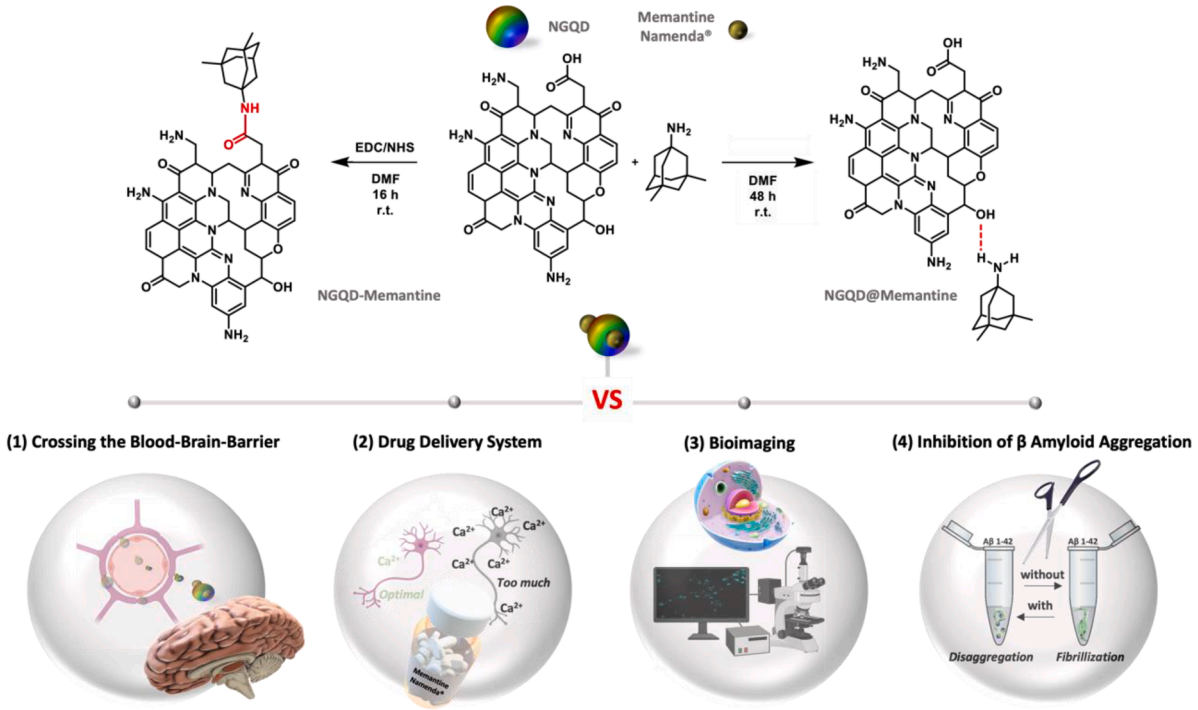

Fig. 1. Schematic illustration of the surface engineering on NGQDs to achieve the multifunctional nanoparticles (*i.e.*, NGQD-Memantine and NGQD@Memantine) and overview of the applications developed in this work. The NGQDs nanoplatform allows (1) permeability across the BBB, (2) the mass fabrication of drug delivery systems and therefore the regulation of NMDA receptors, (3) bioimaging carriers via cytoplasmic staining and, (4) the inhibition of Aβ peptide 1–42 fibrillation. A hypothetical structure, elucidated from the structural characterization of NGQD [33], is illustrated to clarify the amide-bond formation and the non-covalent approach.

87.3 at.%), nitrogen (10.5 and 8.5 at.%), and oxygen (11.3 and 4.2 at.%), for NGQD-Memantine and NGQD@Memantine respectively, (Fig. 2g,h, Figures S3-S6 and Table S1 and S2). The high-resolution nitrogen spectra revealed that the fitted peak area corresponding to O = C—N/N = C increase significantly from 1.3% [33], to 68.9% in NGQDs-Memantine (Fig. 2g and Table S1), verifying the covalent hybrid formation through a carboxyl-to-amine crosslink, in agreement with the FTIR. In contrast, Fig. 2h did not exhibit such an increase (Table S2) since there was no formation of new O = C—N/N = C bonds in the hybrid structure, proving the non-covalent modification. The approximate weight of Memantine bonded to NGQDs, estimated by thermogravimetric analysis (TGA), was significantly higher, 30 ± 2%, for NGQD@Memantine than 18 ± 4% for NGQD-Memantine (Figure S7 and Figure S8), suggesting a better efficiency of the non-covalent process in contrast to the covalent approach. This phenomenon might be ascribed to the many atoms used in the non-covalent approach diverging from the functional groups used in the covalent approach.

The optical properties of the hybrid nanoparticles were assessed in an aqueous solvent. Overall, the UV–Vis absorption spectrum presented a slight shift of the absorption bands in the UV region, compared to pristine dots (Fig. 2i,j and Figure S9). Specifically, the band attributed to the π→π* transition (*i.e.*, C = C bonds) [33] at 288 and 286 nm for the NGQD-Memantine and NGQD@Memantine hybrids, compared to 285 nm from NGQDs, was slightly shifted towards longer wavelengths. Additionally, a red shift was observed for the n→π* transition at 329 and 330 nm for NGQD-Memantine and NGQD@Memantine, respectively, compared to 326 nm of NGQDs. The latter band was assigned to C = O, C = N containing functional groups present in the NGQDs [33]. The fluorescence emission of NGQD-Memantine and NGQD@Memantine showed the excitation-dependent behavior typical of the NGQDs that may arise from different radiative recombination pathways (Fig. 2i,j and Figure S9) [33]. The coupling of the Memantine did not affect the dots emission properties (*i.e.*, excitation-dependent behavior). Nevertheless, a change in the optimal excitation and emission wavelength for the conjugates was observed and suggested a different distribution of emissive sites on each dot after the functionalization (further details, Table S3). All taken together, these data confirm the successful conjugation of the Memantine onto the surface of the dots.

3.2. Multifunctional applications against neurodegenerative diseases

3.2.1. NGQDs rescue Memantine-induced cytotoxicity and regulate NMDA receptors

Fibrous astrocytes C8-D1A and vascular endothelial MSI cell lines were chosen to form the *in vitro* BBB model. Therefore, the cell viability was analyzed in those cell lines to compare the toxicity in the presence of Memantine, NGQDs, NGQD-Memantine, and NGQD@Memantine (Figures S10–13). In both cell lines, NGQDs demonstrated barely toxicity across all concentrations and incubation periods (Figure S10). Similar viability results were already reported for other types of cell lines [32,39,40]. On the contrary, a drop in the viability was observed in Fig. 3a-d related to the systems NGQD-Memantine and NGQD@Memantine at 200 μg/mL, which might be ascribed to the drug Memantine, especially at the highest concentrations (Figure S11). At the incubation time of 24 and 48 h, almost unchanged viability was observed up to a concentration of 100 μg/mL, and a slight decrease was observed during the incubation time (Fig. 3a-d). The cell viability gradually decreased for further increased concentration until a profound reduction to almost zero cell viability. The used concentrations of NGQD-Memantine and NGQD@Memantine were recalculated according to the detected concentration of Memantine in the sample via TGA (Figures S7–8 and Figures S12–13). Currently, the normal reported dosage used in plasma is around 70 to 150 ng/mL [43,44]. This means that higher concentrations were used in our *in vitro* experiments, and we can conclude that up to 20 μg/mL of Memantine loaded onto the nanoparticles barely presented cytotoxicity, *i.e.*, representing safe dosages for the cells used.

Memantine is a clinically used drug, utilize to prevent neuronal cell death induced by excitotoxicity caused by the excessive influx of

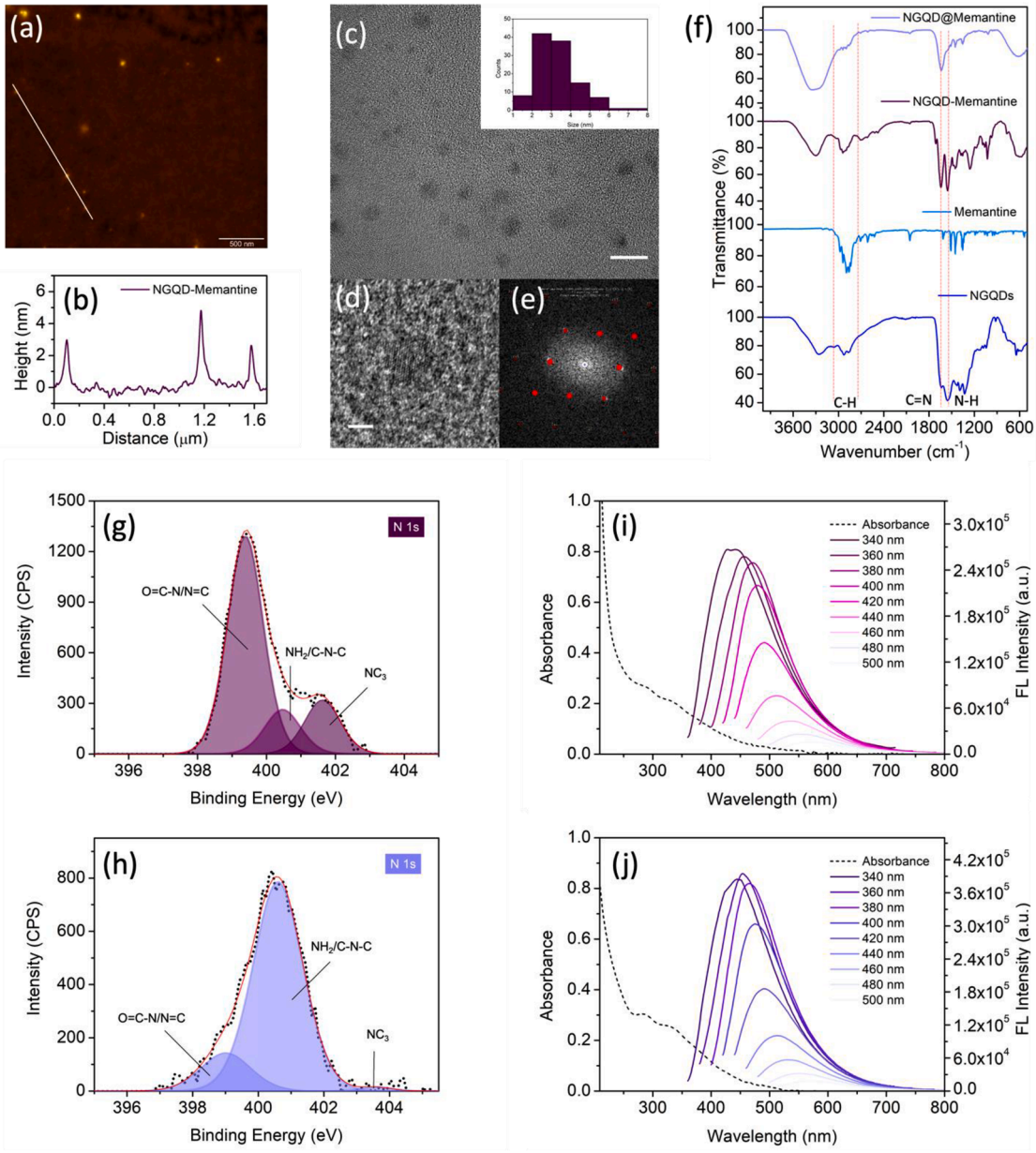

Fig. 2. Morphology, size, structure and optical properties: (a) AFM image of NGQD-Memantine particles and their corresponding (b) height profile along the line, (c) TEM image of NGQD-Memantine (scale bar 10 nm) with size distribution in the inset, (d) HR-TEM (scale bar 2 nm) and corresponding (e) FFT confirming a high crystal quality of the system (hexagonal crystalline structure), (f) FTIR spectra, (g) and (h) high-resolution XPS spectra of N 1 s with chemical bond fitting for NGQD-Memantine and NGQD@Memantine, respectively, (i) and (j) UV–Vis (dash line) and FL emission spectra of NGQD-Memantine and NGQD@Memantine, respectively.

calcium ions due to over-stimulation of glutamate receptors by excessive glutamate [45]. To find out whether the binding of Memantine to NGQDs affects or modifies its function, we investigated the regulation of Ca^{2+} influx in astrocytes since these cells are present in the BBB and express NMDA receptors. The C8-D1A cells were chosen as models for this experiment and the NMDA receptors were activated with a combination of l-Glutamine and l-Glycine [46]. The activation of NMDA receptors resulted in the increased influx of Ca^{2+} ions to the neuronal cells. The C8 D1A cells were pre-stained with Fluo-4 dye, which increased its fluorescence in the presence of Ca^{2+}. Memantine, NGQDs, and their derivatives, *i.e.*, NGQD-Memantine and NGQD@Memantine, were incubated with the Fluo-4 pre-stained astrocytes, and the level of intracellular Ca^{2+} before and after activation of NMDA receptors was compared (Fig. 3e). Notably, it was found that all the treatments significantly decreased the Ca^{2+} influx, *i.e.*, inhibited the effect of NMDA receptors. It indicated that both covalent and non-covalent coupling of Memantine to NGQDs did not modify the pharmaceutical activity of Memantine. While this behavior was expected with free or bound Memantine, we were surprised to observe a similar effect with pristine NGQDs. The exact mechanism is yet to be determined, but reported studies have revealed that certain types of carbon dots can reduce the release of l-glutamate neurotransmitters from axonal vesicles and decrease its uptake [47]. Besides, it was found that carbon dots could inhibit acetylcholine esterase, which operates in neural synapses [48]. Overall, the inhibitory effect of Memantine remains intact when bound to NGQDs and reinforces by the NGQDs side-effect.

3.2.2. *Bioimaging*

Due to the interesting optical properties of the NGQDs, NGDQ@Memantine and NGQD-Memantine were further applied to *in vitro* bioimaging. The NGQD fluorescence was detectable in the cytoplasm of the cells after 24 h of incubation (Figure S14) [28,33,39].

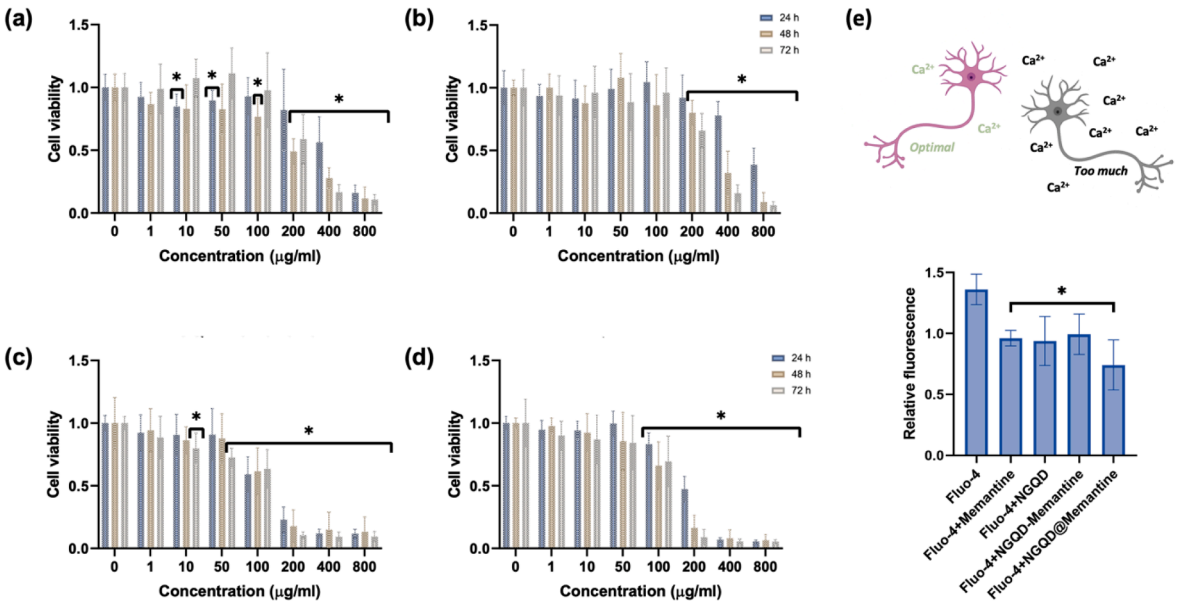

Fig. 3. Cell viability results assessed by the MTT assay: NGQD-Memantine (a) C8-D1A cells and (b) MS1 cell lines. NGQD@Memantine (c) C8 D1A and (b) MS1 cell lines. Data are expressed as mean ± SD ($n = 4$), $^*P < 0.05$ (two-sample unpaired *t*-test). (e) Regulation of NMDA receptors in fibrous astrocytes. Relative fluorescence of C8 D1A cell line pre-stained with Fluo-4 dye, which increased its fluorescence in presence of Ca^{2+}. Data are expressed as mean ± SD ($n = 4$), $^*P < 0.05$ (two-sample unpaired *t*-test).

Similar behavior was observed after the functionalization with Memantine. Fig. 3e,f displayed that the hybrid nanoparticles entered the cells and were situated in the cytoplasm as readily as the NGQDs. The NGQDs and their derivatives might penetrate the cells by endocytosis process via caveolae-mediated and clathrin-mediated pathways, as it was already ascribed to other carbon nanoparticles [49–51]. Nevertheless, the detected fluorescence intensity of hybrid nanoparticles was much lower than pristine NGQDs, due to the surface modification with Memantine (Figure S14 and Fig. 4a,b) [33,52].

3.2.3. *Crossing the BBB*

Testing the permeability of NGQDs and the hybrid NGQDs nanoparticles through an *in vitro* model of the BBB could be performed as a standard migration assay through a layer of co-cultured cells. Nevertheless, utilizing the xCELLigence real-time cell-layer analysis (RTCA) system for the BBB function in 3D models was the key, since it offers real-time cell electronic sensing and provides key information lacking in traditional experiments [53]. Firstly, it was necessary to establish the appropriate density of the selected cell lines (*i.e.*, C8 D1A and MS1). It was done following a modified protocol (Fig. 4c) to ensure that a monolayer of cells with tight junctions was formed when adding the samples (further information in SI and Figure S16) [54]. When the cells reached the plateau phase, as determined by RTCA, the negative control (Streptavidin-Alexa 488) and positive control (Propidium iodide) confirmed the successful formation of the model (Fig. 4b). Notably, 75% of NGQDs permeated through the BBB model, showing a significant increase compared to the positive control (Fig. 4d). Similarly, the passage of NGQD@Memantine through the BBB was about 71%. On

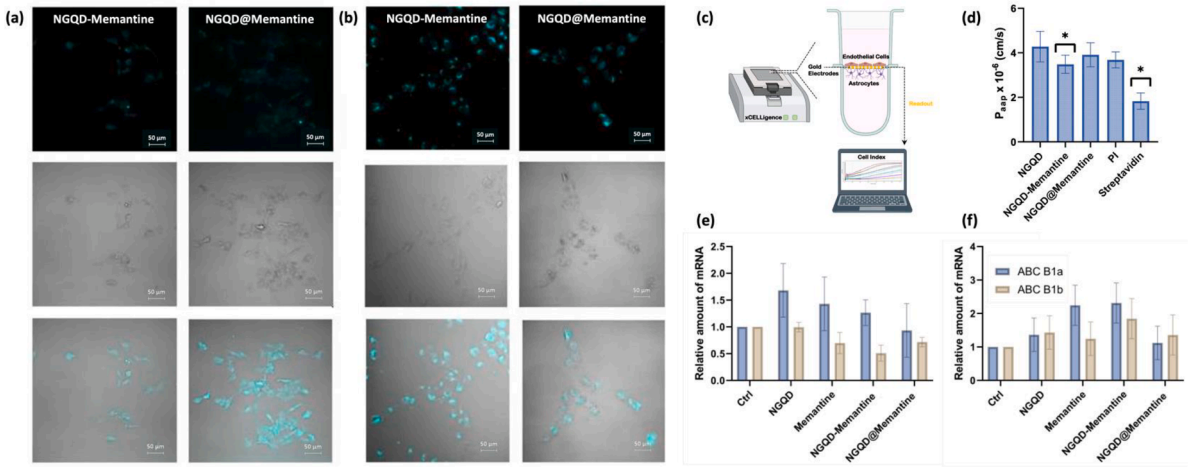

Fig. 4. Confocal fluorescence bioimaging of the cellular internalization: (a) C8-D1A and (b) MS1 cell lines. Corresponding images under bright, fluorescence fields and their corresponding overlay (scale bar 50 μm). Permeability and passage studies through the BBB: (c) Schematic representation of the trans-well culture system used in the *in vitro* BBB model for the xCELLigence device. (d) Apparent permeability coefficients (Papp) of NGQDs, NGQD-Memantine and NGQD@Memantine. Propidium iodide (PI) was set as positive control (*i.e.*, can cross the BBB) and Streptavidin as negative control (*i.e.*, cannot cross the BBB). Data are expressed as mean ± SD ($n = 4$), $^*P < 0.05$ (two-sample unpaired *t*-test). Expression of ABC B1a and ABC B1b transporter's mRNA after incubation with NGQDs and their derivatives in 24 h for (e) C8D1A and (f) MS1 cell lines.

the contrary, a significant reduction was observed compared to the other systems when using NGQD-Memantine (55%, Fig. 4d). The higher passage of NGQD@Memantine compared to NGQD-Memantine may be attributed to the higher toxicity associated with a greater Memantine loading (Fig. 3a-d) and, therefore, a slight violation of BBB integrity. Overall, we proved the ability of the carbon nanoparticles to pass through the BBB model.

The BBB has high levels of expression of ABC transporters in the cell membranes (mainly ABC B1, C1 and G2). Specifically, the ABC transporters are powerful gatekeepers to the brain, which regulate the delivery of small drugs designed to access the central nervous system [55–57]. Therefore, their role was investigated thoroughly choosing the HL-60 cell lines overexpressing ABC transporters as model. By fluorescent NGQD exclusion assay, we found that the NGQDs could be a weak substrate for the ABC B1 transporter because we observed a significantly lower fluorescence compared to the control HL-60 cells non-overexpressing the ABC transporters, and a slight decrease for ABC C1 and ABC G2. Therefore, the NGQDs were partially effluxed from the ABC B1 overexpressing cells (further details in SI and Figure S16). Notably, the ABC B1 expression is known to be stimulated by drugs [58, 59]. Thus, we aimed to assess whether the NGQDs functionalized with Memantine affect the level of the mRNA genes ABC B1a and B1b in the cells used in the BBB model. In Fig. 4e,f, it was noted a slight increase in ABC B1 gene expression following treatment with hybrid nanoparticles, particularly when it was used NGQDs, which is not a drug itself. This increase was most significant in ABC B1a, which exhibits higher expression in the BBB.

Overall, Memantine itself is not a substrate of any of the three most important ABC transporters in the BBB [60]. Nevertheless, Memantine is able to cross the BBB by acting as a substrate of the Solute Carrier transporters (SLC22A), which allow it to enter the central nervous system [60]. Then, taking into account the permeability results from the real-time cell electronic sensing (Fig. 4d) and the fluorescence exclusion assay of the ABC transporters (Fig. 4e,f), it can be concluded that the potential efficiency of NGQD and its derivatives to cross the cell membranes forming BBB was not considerably affected by the ABC transporters. Thereby, additional mechanisms such as passive diffusion or endocytosis might be involved when the dots cross the blood-brain barrier.

3.2.4. The effect of NGQD-based hybrid nanoparticles on the process of Aβ1–42 peptides fibrillation

Neuronal damage may be caused by protein aggregation, and in particular, the Aβ1–42 peptide is the most common variant in human cerebrospinal fluid and is the main component of amyloid plaques [61]. Therefore, the potential of the pristine NGQDs for inhibiting Aβ peptide aggregation was investigated by performing AFM. The Aβ1–42 fibers during the fibrillation process were measured at an optimal time of 7 days (Fig. 5). During fibrillation, mature fibers were observed without the NGQDs (Fig. 5Aβ1–42, control sample). Contrarily, the mature fibers were not observed in the presence of the pristine NGQDs and the NGQDs-based hybrids. Instead, oligomers of these fibers were observed, constituting 0.4% for NGQDs, 1.69% for NGQD-Memantine, and 2.7% for NGQD@Memantine of the total image area from Fig. 5, suggesting that the materials were able to inhibit the growth of the mature fibers even in the shortest time. Some authors have already described that the mature fibers are stabilized by hydrophobic and hydrogen-bonding interactions within the β-sheets that form their core [62]. Besides, some carbon-based dots were already proven to interact with amyloid fibers [36,37]. Thus, we might ascribe the inhibition of the fibrillation to the formation of new interactions between the oligomers and the protofibrils of the β-sheets within the NGQDs materials and, therefore, their instability and, finally, the inhibition.

4. Conclusions

In this work, we have made valuables insights into the use of NGQDs for potential treatment of neurodegenerative diseases, with multiple benefits. Firstly, we have synthesized and characterized a multifunctional material based on NGQDs and Memantine using the covalent and non-covalent approaches. From our results we have understood that the pharmaceutical activity of Memantine was not altered by surface interactions neither using covalent approaches, suggesting that both techniques are useful, and neither exhibits a hierarchical advantage in terms of specificity. Nevertheless, the non-covalent approach might be more suitable due to a feasible synthetic procedure. Secondly, we have demonstrated with a detailed real-time experiment that the NGQDs and the as-prepared systems were able to cross the BBB and the essential ABC transporters of the BBB did not considerably affect the ability of the dots to cross the BBB. Thirdly and surprisingly, pristine NGQDs have significant implications regulating $Ca^{2+}$and showed similar effect to the well-known neurodegenerative drug Memantine. Lastly, the Aβ1–42 peptides are the most common variant in human cerebrospinal fluid and is the main component of amyloid plaques and its inhibition was assed using NGQDs and its derivatives at an optimal time of 7 days confirmed by AFM. This inhibition could be ascribed to the formation of new interactions between the oligomers and the protofibrils of the β-sheets within the NGQDs materials and, therefore, their instability. Considering all these findings and the potential demonstrated as bioimaging carriers against various cell lines, it is not surprising that the development of new therapeutic nanoparticles based on GQDs is underway. This holds promise for broader applicability—an extension to using other molecules and drugs for the treatment of brain tumors or related diseases within the central nervous system.

CRediT authorship contribution statement

I. Jénnifer Gómez: Conceptualization, Methodology, Visualization, Writing – original draft, Writing – review & editing, Funding acquisition. **Petra Křížková:** Methodology, Visualization, Writing – review &

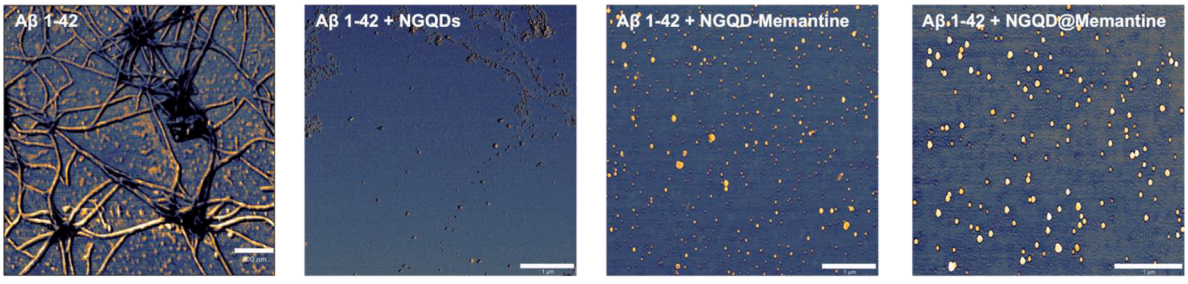

Fig. 5. AFM phase images of Aβ1–42 peptides before and after treatment with NGQDs, NGQD-Memantine and NGQD@Memantine. All the experiments were incubated at 37°C for 7 days. The Aβ1–42 image correspond to the control sample and showed a mat of mature amyloid fibers. The rest of the figures are the ones treated with NGQDs, NGQD-Memantine and NGQD@Memantine, respectively. The AFM images displayed much shortened aggregates, which correspond with oligomers of the amyloid fibers. Scales (200 nm - 1 μm).

editing. **Anna Dolečková:** Methodology, Visualization, Writing – review & editing. **Lucía Cardo:** Methodology, Visualization, Writing – review & editing. **Cecilia Wetzl:** Methodology, Visualization, Writing – review & editing. **Naděžda Pizúrová:** Methodology, Visualization, Writing – review & editing. **Maurizio Prato:** Supervision, Writing – review & editing, Funding acquisition. **Jiřina Medalová:** Supervision, Conceptualization, Methodology, Validation, Visualization, Writing – original draft, Writing – review & editing. **Lenka Zajíčková:** Supervision, Conceptualization, Writing – review & editing, Funding acquisition.

Declaration of competing interest

The authors declare that they have no competing financial interests or personal relationships that could have appeared to influence the work reported in this paper.

Data availability

Data will be made available on request.

Acknowledgment

This work was supported by Operational Program Research, Development, and Education-Project 'MSCAfellow4@MUNI' (No. CZ.02.2.69/0.0/0.0/20_079/0017045). The Spanish Ministry of Universities is acknowledged for a Beatriz Galindo (BG22/000147) and Maria Zambrano funding (RSU.UDC.MZ09) transferred by the European Union-Next GenerationEU. We acknowledge CzechNanoLab Research Infrastructure (LM2018110), supported by the Ministry of Education, Youth and Sports of the Czech Republic (MEYS CR). We are grateful to Prof. Vladimír Šindelář and Prof. Petr Klan for allowing us to use the MW reactor, UV–Vis and fluorescence spectrometer, supported by RECETOX research infrastructure (via MEYS CR under LM2018121). M.P. is AXA Professor and is supported by the European Research Council (ERC-AdG-2019, N. 885323), the Agencia Estatal de Investigación-AEI ("Proyectos I+D+I 2019 -Modalidad Retos Investigación", N. PID2019–108523RB-I00), by Grant PRE2020–095099.

Supplementary materials

Supplementary material associated with this article can be found, in the online version, at doi:10.1016/j.apmt.2024.102072.

References

[1] L. Gan, M.R. Cookson, L. Petrucelli, A.R. La Spada, Converging pathways in neurodegeneration, from genetics to mechanisms, Nat. Neurosci. 21 (2018) 1300–1309, https://doi.org/10.1038/s41593-018-0237-7.

[2] J.P. Taylor, J. Hardy, K.H. Fischbeck, Toxic proteins in neurodegenerative disease, Science (1979)Science (1979) 296 (2002) (1979) 1991–1995, https://doi.org/10.1126/science.1067122.

[3] A.L. Sheldon, M.B. Robinson, The role of glutamate transporters in neurodegenerative diseases and potential opportunities for intervention, Neurochem. Int. 51 (2007) 333–355.

[4] M.A. Rogawski, G.L. Wenk, The neuropharmacological basis for the use of memantine in the treatment of Alzheimer's disease, CNS. Drug Rev. 9 (2003) 275–308, https://doi.org/10.1111/j.1527-3458.2003.tb00254.x.

[5] C.D. Pereira, F. Martins, J. Wiltfang, O.A.B. Da Cruz E Silva, S. Rebelo, ABC transporters are key players in Alzheimer's disease, J. Alzheimer's Disease 61 (2017) 463–485, https://doi.org/10.3233/JAD-170639.

[6] G. Guillama Barroso, M. Narayan, M. Alvarado, I. Armendariz, J. Bernal, X. Carabaza, S. Chavez, P. Cruz, V. Escalante, S. Estorga, D. Fernandez, C. Lozano, M. Marrufo, N. Ahmad, S. Negrete, K. Olvera, X. Parada, B. Portillo, A. Ramirez, R. Ramos, V. Rodriguez, P. Rojas, J. Romero, D. Suarez, G. Urueta, S. Viel, Nanocarriers as potential drug delivery candidates for overcoming the blood-brain barrier: challenges and possibilities, ACS. Omega 5 (2020) 12583–12595, https://doi.org/10.1021/acsomega.0c01592.

[7] T.K. Henna, V.R. Raphey, R. Sankar, V.K. Ameena Shirin, H.V. Gangadharappa, K. Pramod, Carbon nanostructures: the drug and the delivery system for brain disorders, Int. J. Pharm. 587 (2020) 119701, https://doi.org/10.1016/j.ijpharm.2020.119701.

[8] B.S. Wong, S.L. Yoong, A. Jagusiak, T. Panczyk, H.K. Ho, W.H. Ang, G. Pastorin, Carbon nanotubes for delivery of small molecule drugs, Adv. Drug Deliv. Rev. 65 (2013) 1964–2015, https://doi.org/10.1016/j.addr.2013.08.005.

[9] H. Li, Y. Luo, P. Derreumaux, G. Wei, Carbon nanotube inhibits the formation of β-sheet-rich oligomers of the Alzheimer's amyloid-β(16-22) peptide, Biophys. J. 101 (2011) 2267–2276, https://doi.org/10.1016/j.bpj.2011.09.046.

[10] X. Ma, L. Zhong, H. Guo, Y. Wang, N. Gong, Y. Wang, J. Cai, X.J. Liang, Multiwalled carbon nanotubes induced hypotension by regulating the central nervous system, Adv. Funct. Mater. 28 (2018) 1–9, https://doi.org/10.1002/adfm.201705479.

[11] H. Kafa, J.T.W. Wang, N. Rubio, K. Venner, G. Anderson, E. Pach, B. Ballesteros, J. E. Preston, N.J. Abbott, K.T. Al-Jamal, The interaction of carbon nanotubes with an invitro blood-brain barrier model and mouse brain invivo, Biomaterials 53 (2015) 437–452, https://doi.org/10.1016/j.biomaterials.2015.02.083.

[12] Y. Liu, Y. Zhao, B. Sun, C. Chen, Understanding the toxicity of carbon nanotubes, Acc. Chem. Res. 46 (2013) 702–713, https://doi.org/10.1021/ar300028m.

[13] A.P. Francis, T. Devasena, Toxicity of carbon nanotubes: a review, Toxicol. Ind. Health 34 (2018) 200–210, https://doi.org/10.1177/0748233717747472.

[14] A.A. John, A.P. Subramanian, M.V. Vellayappan, A. Balaji, H. Mohandas, S. K. Jaganathan, Carbon nanotubes and graphene as emerging candidates in neuroregeneration and neurodrug delivery, Int. J. Nanomedicine 10 (2015) 4267–4277, https://doi.org/10.2147/IJN.S83777.

[15] M.C.P. Mendonça, E.S. Soares, M.B. de Jesus, H.J. Ceragioli, M.S. Ferreira, R. R. Catharino, M.A. da Cruz-Höfling, Reduced graphene oxide induces transient blood-brain barrier opening: an *in vivo* study, J. Nanobiotechnology. 13 (2015) 1–13, https://doi.org/10.1186/s12951-015-0143-z.

[16] B. Pakhira, M. Ghosh, A. Allam, S. Sarkar, Carbon nano onions cross the blood brain barrier†, RSC. Adv. 6 (2016) 29779–29782, https://doi.org/10.1039/C5RA23534K.

[17] M.E. Plonska-Brzezinska, Carbon nano-onions: a review of recent progress in synthesis and applications, ChemNanoMat. 5 (2019) 568–580, https://doi.org/10.1002/cnma.201800583.

[18] H. Wu, Q. Huang, Y. Tan, Carbon nanomaterials for biomedical applications, Carbon Nanomater.: Model., Des. Appl (2019) 255–293, https://doi.org/10.1201/9781351123587-7.

[19] A. Cayuela, M.L. Soriano, C. Carrillo-Carrión, M. Valcárcel, Semiconductor and carbon-based fluorescent nanodots: the need for consistency, Chem. Commun. 52 (2016) 1311–1326, https://doi.org/10.1039/C5CC07754K.

[20] L. Đorđević, F. Arcudi, M. Cacioppo, M. Prato, A multifunctional chemical toolbox to engineer carbon dots for biomedical and energy applications, Nat. Nanotechnol. 17 (2022) 112–130, https://doi.org/10.1038/s41565-021-01051-7.

[21] Z. Kang, B. Yang, M. Prato, Carbon Nanodots: nanolights Illuminating a Bright Future, Small 19 (2023) e2304703, https://doi.org/10.1002/smll.202304703.

[22] D. Qu, Z. Sun, The formation mechanism and fluorophores of carbon dots synthesized: via a bottom-up route, Mater. Chem. Front. 4 (2020) 400–420, https://doi.org/10.1039/c9qm00552h.

[23] F. Arcudi, L. Đorđević, M. Prato, Design, synthesis, and functionalization strategies of tailored carbon nanodots, Acc. Chem. Res. 52 (2019) 2070–2079, https://doi.org/10.1021/acs.accounts.9b00249.

[24] X. Xu, R. Ray, Y. Gu, H.J. Ploehn, L. Gearheart, K. Raker, W.A. Scrivens, Electrophoretic analysis and purification of fluorescent single-walled carbon nanotube fragments, J. Am. Chem. Soc. 126 (2004) 12736–12737, https://doi.org/10.1021/ja040082h.

[25] S.Y. Lim, W. Shen, Z. Gao, Carbon quantum dots and their applications, Chem. Soc. Rev. 44 (2014) 362–381, https://doi.org/10.1039/c4cs00269e.

[26] X.T. Zheng, A. Ananthanarayanan, K.Q. Luo, P. Chen, Glowing graphene quantum dots and carbon dots: properties, syntheses, and biological applications, Small. 11 (2015) 1620–1636, https://doi.org/10.1002/smll.201402648.

[27] J. Liu, R. Li, B. Yang, Carbon dots: a new type of carbon-based nanomaterial with wide applications, ACS. Cent. Sci. 6 (2020) 2179–2195, https://doi.org/10.1021/acscentsci.0c01306.

[28] I.J. Gómez, M. Vázquez Sulleiro, A. Dolečková, N. Pizúrová, J. Medalová, A. Bednařík, J. Preisler, D. Nečas, L. Zajíčková, Structure elucidation of multicolor emissive graphene quantum dots towards cell guidance, Mater. Chem. Front. 6 (2022) 145–154, https://doi.org/10.1007/978-1-4020-6120-2.

[29] G. Ge, L. Li, D. Wang, M. Chen, Z. Zeng, W. Xiong, X. Wu, C. Guo, Carbon dots: synthesis, properties and biomedical applications, J. Mater. Chem. B 9 (2021) 6553–6575, https://doi.org/10.1039/d1tb01077h.

[30] E.S. Seven, Y.B. Seven, Y. Zhou, S. Poudel-Sharma, J.J. Diaz-Rucco, E. Kirbas Cilingir, G.S. Mitchell, J.D. Van Dyken, R.M. Leblanc, Crossing the blood–brain barrier with carbon dots: uptake mechanism and *in vivo* cargo delivery, Nanoscale Adv. 3 (2021) 3942–3953, https://doi.org/10.1039/d1na00145k.

[31] W. Zhang, G. Sigdel, K.J. Mintz, E.S. Seven, Y. Zhou, C. Wang, R.M. Leblanc, Carbon dots: a future blood–brain barrier penetrating nanomedicine and drug nanocarrier, Int. J. Nanomedicine 16 (2021) 5003–5016, https://doi.org/10.2147/IJN.S318732.

[32] I.J. Gómez, K. Ovejero-Paredes, J.M. Méndez-Arriaga, N. Pizúrová, M. Filice, L. Zajíčková, S. Prashar, S. Gómez-Ruiz, Organotin(IV)-Decorated Graphene Quantum Dots as Dual Platform for Molecular Imaging and Treatment of Triple Negative Breast Cancer, Chemistry (2023), https://doi.org/10.1002/chem.202301845.

[33] I.J. Gómez, M. Vázquez Sulleiro, A. Dolečková, N. Pizúrová, J. Medalová, R. Roy, D. Nečas, L. Zajíčková, Exploring the emission pathways in nitrogen-doped

graphene quantum dots for bioimaging, J. Phys. Chem. C 125 (2021) 21044–21054, https://doi.org/10.1021/acs.jpcc.1c06029.
[34] H.A. Sansing, N.A. Renner, A.G. MacLean, An inverted blood-brain barrier model that permits interactions between glia and inflammatory stimuli, J. Neurosci. Methods 207 (2012) 91–96, https://doi.org/10.1016/j.jneumeth.2012.03.015.
[35] S. Hanada, K. Fujioka, Y. Inoue, F. Kanaya, Y. Manome, Cell-based in vitro blood – brain barrier model can rapidly evaluate nanoparticles ' Brain permeability in association with particle size and surface modification, Int. J. Mol. Sci. 15 (2014) 1812–1825, https://doi.org/10.3390/ijms15021812.
[36] D. Kim, J.M. Yoo, H. Hwang, J. Lee, S.H. Lee, S.P. Yun, M.J. Park, M.J. Lee, S. Choi, S.H. Kwon, S. Lee, S.H. Kwon, S. Kim, Y.J. Park, M. Kinoshita, Y.H. Lee, S. Shin, S. R. Paik, S.J. Lee, S. Lee, B.H. Hong, H.S. Ko, Graphene quantum dots prevent α-synucleinopathy in Parkinson's disease, Nat. Nanotechnol. 13 (2018) 812–818, https://doi.org/10.1038/s41565-018-0179-y.
[37] Y. Liu, L.P. Xu, W. Dai, H. Dong, Y. Wen, X. Zhang, Graphene quantum dots for the inhibition of β amyloid aggregation, Nanoscale 7 (2015) 19060–19065, https://doi.org/10.1039/c5nr06282a.
[38] D. Nečas, P. Klapetek, Gwyddion: an open-source software for SPM data analysis, Central Europ. J. Phys 10 (2012) 181–188, https://doi.org/10.2478/s11534-011-0096-2.
[39] I.J. Gómez, M. Russo, O.A. Arcidiacono, E.M. Sanchez-Carnerero, P. Klan, L. Zajıckova, Coupling BODIPY with nitrogen-doped graphene quantum dots to address the water solubility of, Mater. Chem. Front. 6 (2022) 1719–1726, https://doi.org/10.1039/d2qm00200k.
[40] I.J. Gomez, B. Arnaiz, M. Cacioppo, F. Arcudi, M. Prato, Nitrogen-doped Carbon Nanodots for bioimaging and delivery of paclitaxel, J. Mater. Chem. B 6 (2018) 5540–5548, https://doi.org/10.1039/c8tb01796d.
[41] I.J. Gómez, M. Díaz-Sánchez, N. Pizúrová, L. Zajíčková, S. Prashar, S. Gómez-Ruiz, Crystalline F-doped titanium dioxide nanoparticles decorated with graphene quantum dots for improving the photodegradation of water pollutants, J. Photochem. Photobiol. a Chem. 443 (2023) 114875, https://doi.org/10.1016/j.jphotochem.2023.114875.
[42] F. Arcudi, L. Đorđević, Supramolecular chemistry of carbon-based dots offers widespread opportunities, Small. (2023), https://doi.org/10.1002/smll.202300906.
[43] C.G. Parsons, A. Stöffler, W. Danysz, Memantine: a NMDA receptor antagonist that improves memory by restoration of homeostasis in the glutamatergic system - too little activation is bad, too much is even worse, Neuropharmacology 53 (2007) 699–723, https://doi.org/10.1016/j.neuropharm.2007.07.013.
[44] M. Trotman, P. Vermehren, C.L. Gibson, R. Fern, The dichotomy of memantine treatment for ischemic stroke: dose-dependent protective and detrimental effects, J. Cerebral Blood Flow Metabol 35 (2015) 230–239, https://doi.org/10.1038/jcbfm.2014.188.
[45] Z. Liu, X. Qiu, S. Mak, B. Guo, S. Hu, J. Wang, F. Luo, D. Xu, Y. Sun, G. Zhang, G. Cui, Y. Wang, Z. Zhang, Y. Han, Multifunctional memantine nitrate significantly protects against glutamate-induced excitotoxicity via inhibiting calcium influx and attenuating PI3K/Akt/GSK3beta pathway, Chem. Biol. Interact. 325 (2020), https://doi.org/10.1016/j.cbi.2020.109020.
[46] K. Skowrońska, M. Obara-Michlewska, M. Zielińska, J. Albrecht, NMDA receptors in astrocytes: in search for roles in neurotransmission and astrocytic homeostasis, Int. J. Mol. Sci. 20 (2019), https://doi.org/10.3390/ijms20020309.
[47] T. Borisova, A. Nazarova, M. Dekaliuk, N. Krisanova, N. Pozdnyakova, A. Borysov, R. Sivko, A.P. Demchenko, Neuromodulatory properties of fluorescent carbon dots: effect on exocytotic release, uptake and ambient level of glutamate and GABA in brain nerve terminals, Int. J. Biochem. Cell Biol. 59 (2015) 203–215, https://doi.org/10.1016/j.biocel.2014.11.016.
[48] S.S. Suner, M. Sahiner, R.S. Ayyala, V.R. Bhethanabotla, N. Sahiner, Nitrogen-Doped Arginine Carbon Dots and Its Metal Nanoparticle Composites as Antibacterial Agent, C—J. Carbon Res 6 (2020) 58, https://doi.org/10.3390/c6030058.
[49] Y. Wei, X. Jin, T. Kong, W. Zhang, B. Zhu, The endocytic pathways of carbon dots in human adenoid cystic carcinoma cells, Cell Prolif. 52 (2019), https://doi.org/10.1111/cpr.12586.
[50] B. Kang, S. Chang, Y. Dai, D. Yu, D. Chen, Cell response to carbon nanotubes: size-dependent intracellular uptake mechanism and subcellular fate, Small. 6 (2010) 2362–2366, https://doi.org/10.1002/smll.201001260.
[51] N. Zhou, S. Zhu, S. Maharjan, Z. Hao, Y. Song, X. Zhao, Y. Jiang, B. Yang, L. Lu, Elucidating the endocytosis, intracellular trafficking, and exocytosis of carbon dots in neural cells, RSC. Adv. 4 (2014) 62086–62095, https://doi.org/10.1039/c4ra09525a.
[52] Q. Zhang, R. Wang, B. Feng, X. Zhong, K.(Ken) Ostrikov, Photoluminescence mechanism of carbon dots: triggering high-color-purity red fluorescence emission through edge amino protonation, Nat. Commun. 12 (2021), https://doi.org/10.1038/s41467-021-27071-4.
[53] K. Solly, X. Wang, X. Xu, B. Strulovici, W. Zheng, Application of real-time cell electronic sensing (RT-CES) technology to cell-based assays, 2004.
[54] Y.A. Abassi, B. Xi, W. Zhang, P. Ye, S.L. Kirstein, M.R. Gaylord, S.C. Feinstein, X. Wang, X. Xu, Kinetic cell-based morphological screening: prediction of mechanism of compound action and off-target effects, Chem. Biol. 16 (2009) 712–723, https://doi.org/10.1016/j.chembiol.2009.05.011.
[55] G. Sita, P. Hrelia, A. Tarozzi, F. Morroni, P-glycoprotein (ABCB1) and oxidative stress: focus on Alzheimer⇔s disease, Oxid. Med. Cell Longev. (2017) 2017, https://doi.org/10.1155/2017/7905486.
[56] W. Löscher, H. Potschka, Blood-brain barrier active efflux transporters: ATP-Binding cassette Gene family, NeuroRx 2 (2005) 86–98.
[57] D.S. Miller, Regulation of ABC transporters at the blood–brain barrier, Clin. Pharmacol. Ther 97 (2015) 395–403, https://doi.org/10.1002/CPT.64.
[58] K. Katayama, K. Noguchi, Y. Sugimoto, Regulations of P-Glycoprotein/ABCB1/MDR1 in human cancer cells, New. J. Sci. 2014 (2014) 1–10, https://doi.org/10.1155/2014/476974.
[59] S. Vautier, C. Fernandez, ABCB1: the role in Parkinson's disease and pharmacokinetics of antiparkinsonian drugs, Expert. Opin. Drug Metab. Toxicol. 5 (2009) 1349–1358, https://doi.org/10.1517/17425250903193079.
[60] K.L. Nilles, E.I. Williams, R.D. Betterton, T.P. Davis, P.T. Ronaldson, Blood–brain barrier transporters: opportunities for therapeutic development in ischemic stroke, Int. J. Mol. Sci. 23 (2022), https://doi.org/10.3390/ijms23031898.
[61] A.E. Roher, J.D. Lowensont, S. Clarket, A.S. Woods, R.J. Cotter, E. Gowing, M.J. Ball, Beta-Amyloid-(1-42)is a major component of cerebrovascular amyloid deposits: implications for the pathology of Alzheimer disease (cerebrovasculature/blood brain barrier), 1993.
[62] O.S. Makin, L.C. Serpell, Structures for amyloid fibrils, FEBS J 272 (2005) 5950–5961, https://doi.org/10.1111/j.1742-4658.2005.05025.x.